ARTICLES

EPR, ENDOR, and optical-absorption study of Cr^{3+} centers substituting for niobium in Li-rich lithium niobate crystals

V. Grachev* and G. Malovichko†
Department of Physics, Osnabrück University, Barbarastr. 7, 49069 Osnabrück, Germany, and Institute for Problems of Material Sciences, National Academy of Sciences, Kiev, Ukraine
(Received 6 January 2000; revised manuscript received 3 May 2000)

A triplet of EPR lines with a relatively small zero-field splitting and a ratio of peak-to-peak intensities of 1:50:1 was found in lithium niobate crystals grown from the melt, with the addition of potassium and of 1 wt % of Cr. Detailed investigations of the angular dependencies of EPR and electron nuclear double-resonance (ENDOR) spectra, the temperature dependence of EPR spectra, and optical absorption allowed us to attribute this triplet to a family of Cr^{3+} centers with $g=1.995\pm0.005$, $|b_2^0|\approx0.0215\pm0.001\ cm^{-1}$, and an optical band at 530 nm. Since strong hyperfine interactions of chromium electrons with the nearest Li nuclei were found by ENDOR, it was concluded that Cr in this center substitutes for Nb. Several hydrogen lines were detected in ENDOR spectra. This sheds light on one of the mechanisms of local charge compensation of the centers. The second possible mechanism—charge compensation by additional Li ions in structural vacancies Li_v^+—is also considered. The members of the family of Cr_{Nb} centers differ from each other by the location of one or both of these compensating defects. An estimation of crystal-field parameters for the observed low-symmetry exchange pairs in nonstoichiometric crystals shows that they consist of $Cr^{3+}_{Li^+}$-$Cr^{3+}_{Li^+}$ centers ''glued'' by the intrinsic defects, but not of self-compensated $Cr^{3+}_{Li^+}$-$Cr^{3+}_{Nb^{5+}}$ centers.

INTRODUCTION

For many years lithium niobate (LN) has been of great interest for both fundamental science and applications, because of the unusual richness of its physical properties.[1,2] Conventional LN crystals, grown from a congruent melt with a lithium deficiency ($X_{melt}=X_{crystal}\approx48.4\%$, where $X=[Li]/([Li]+[Nb])$), contain some percentage of intrinsic (nonstoichiometric) defects. Due to the high concentration of these defects, the congruent crystals are very tolerant to divalent (Me^{2+}) or trivalent (Me^{3+}) impurities, substituting for Li^+ or Nb^{5+}, because the necessary charge compensators (local or distant) can easily be found among the nonstoichiometric defects.

A decrease of the concentration of intrinsic defects caused by using melts with excess[3,4] Li, or by a post-growth vapor transport equilibration (VTE) treatment,[5] leads to essential changes of the conditions for impurity incorporation to the LN, and as a consequence to changes of crystal properties and characteristics (see, for examples Refs. 6 and 7). Even stronger changes were observed[8–10] for crystals grown under special conditions, from melts to which potassium was added (later on labeled $LN_{(K)}$). It was found that they have even lower intrinsic defect concentrations and that potassium does not enter the crystal. Besides the main Fe^{3+} center (where the parameter of the axial crystal field b_2^0 is equal to 0.1768 cm^{-1}) two new iron axial centers (with much lower parameters $b_2^0=0.0495$ and 0.0688 cm^{-1}) have been discovered[11] in $LN_{(K)}$. The difference in their characteristics reflects the different surroundings and structure of these centers.

Results of the first studies of samples with a high Li content (with a ratio $X_{crystal}$ close to 50%), often conventionally called stoichiometric, pushed many laboratories in the world to produce such crystals by different growth techniques,[12–15] and to investigate their properties. Many interesting features were observed,[16–19] initiating the booming interest in these materials.

Detailed investigations of Cr^{3+} centers in LN over a wide range of crystal compositions, doped with various chromium concentrations,[20] have shown that in addition to the main axial chromium center (with $b_2^0=-0.387\ cm^{-1}$, i.e., with a zero-field splitting $\Delta=0.764\ cm^{-1}$, center No. 1), there are several axial and low-symmetry centers with $\Delta\approx0.7-0.87\ cm^{-1}$. Since all these satellite centers disappear in stoichiometric crystals, they were interpreted as complexes, consisting of Cr and nonstoichiometric defects in the nearest or next-nearest cation shells of the impurity surrounding (center Nos. 2–9).

Here we report the results of our study of a Cr^{3+} center with a very low zero-field splitting (No. 10), which was found in crystals grown with an addition of 1 wt % chromium to the $LN_{(K)}$ melt. Radiospectroscopic methods—electron paramagnetic resonance (EPR) and electron nuclear double resonance (ENDOR)—have been applied as our main techniques, since they are very sensitive and informative tools for the study of defect structure and hyperfine interactions. For complementary characterizations, data of optical spectroscopy were also employed.

I. CRYSTALS, EQUIPMENT, COMPUTER PROGRAMS

Special series of the samples, grown by the Czochralski method from melts with different chromium concentrations

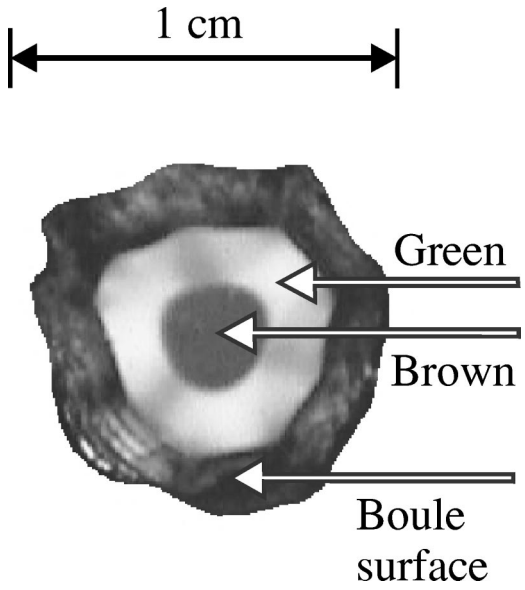

FIG. 1. A cross section of the $LN_{(K)}$ crystal boule grown with an addition of 1 wt % of Cr to the melt. The view is along the *c*-axis of the crystal.

(0.002–1.0 wt %) and different X_{melt} ratios (43–60 %) were used. One further set of crystals with different chromium contents was grown from a congruent melt with the addition of potassium under special conditions, leading to Li-rich samples. The actual composition of crystals X_C was determined by the analysis of the EPR and NMR linewidths and the intensity ratios of the forbidden and allowed resonance transitions.[21,22] $LN_{(K)}$ crystals may possess an $X_{crystal}$ of about 50.0%. Moreover, these samples are close to the regularly ordered crystal (ROC; see the definition and the analysis of crystal composition in Ref. 22). Several chromium-doped samples from different sources were also studied for comparison.

The EPR and ENDOR measurements were carried out in the temperature range 4.2–300 K by means of a Bruker ESR-200 D-SRO with ESP 360 DICE ENDOR system, operating in the *X* band. The study of EPR at 77–950 K was made with a RE-1307 spectrometer at the *Q* band. Optical-absorption spectra were measured using a Bruins Instruments Omega 10/20 spectrometer.

The treatment of the EPR and ENDOR spectra (filtering, peak picking, simulations, spectra subtraction, etc.) and their angular dependencies could only be exploited using advanced numerical methods. For this purpose the ''visual EPR'' and, ''visual ENDOR'' program packages[23] were used. The determination of the relevant spin Hamiltonian parameters of paramagnetic centers was made by a fitting procedure, based on an exact diagonalization of the corresponding matrices.

II. VISUAL OBSERVATION, OPTICAL ABSORPTION

Chromium-doped congruent LN crystals usually have a homogeneous coloration from light green to dark green (depending on the Cr concentration). $LN_{(K)}$ crystals have a similar coloration if the Cr concentration in the melt is less than 0.25 wt %. However, in a $LN_{(K)}$ crystal grown with an additional 1 wt % of Cr in the melt, a very picturesque inhomogeneous coloration of the boule was observed (Fig. 1). The visible three-ray brown star reflects the crystal symmetry.

To investigate a reason for this unusual coloration, two samples from the brown and green parts were cut out (labeled $LN_{(K)}$-brown and $LN_{(K)}$-green below). X-ray single-crystal analysis of both parts showed no visible deviation from the lattice structure of conventional LN ($R3c$ space group symmetry). The spectra of the optical absorption of congruent and $LN_{(K)}$ samples are presented in Fig. 2. An observed strong blueshift of the fundamental absorption edge for $LN_{(K)}$ doped with 0.01 and 0.1 wt % of Cr reflects a decrease of the intrinsic defect content in $LN_{(K)}$ crystals at a low level of chromium dopants.

Optical absorption in both $LN_{(K)}$ samples grown from the melt, with 1 wt % of Cr is comparable to the absorption of a congruent crystal grown with an addition to the melt of 0.02 wt % of Cr only. This means that the coefficient of Cr incorporation for $LN_{(K)}$ crystals is much less than that for congruent crystals.

Three broad bands centered at approximately 340, 490, and 660 nm definitely increase with the rise of Cr concentra-

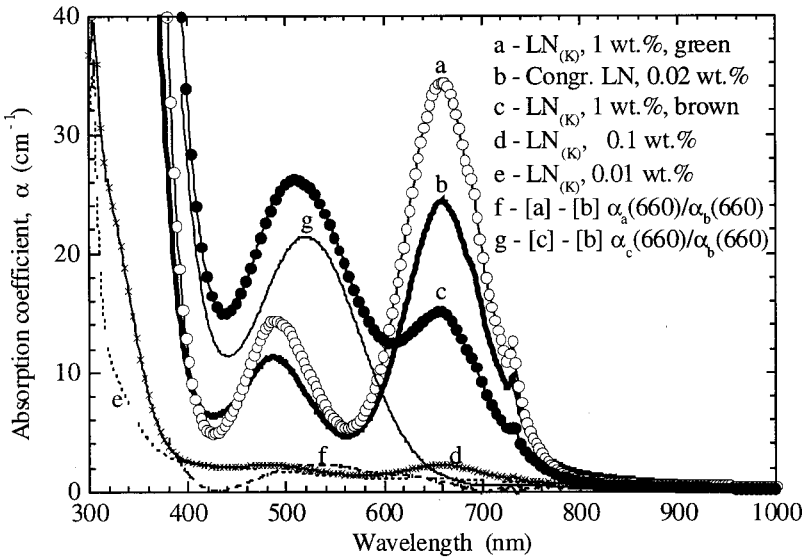

FIG. 2. Optical-absorption spectra of Cr-doped crystals at room temperature. The light propagation is along the **y** axis, and the light polarization is **E**∥**z**.

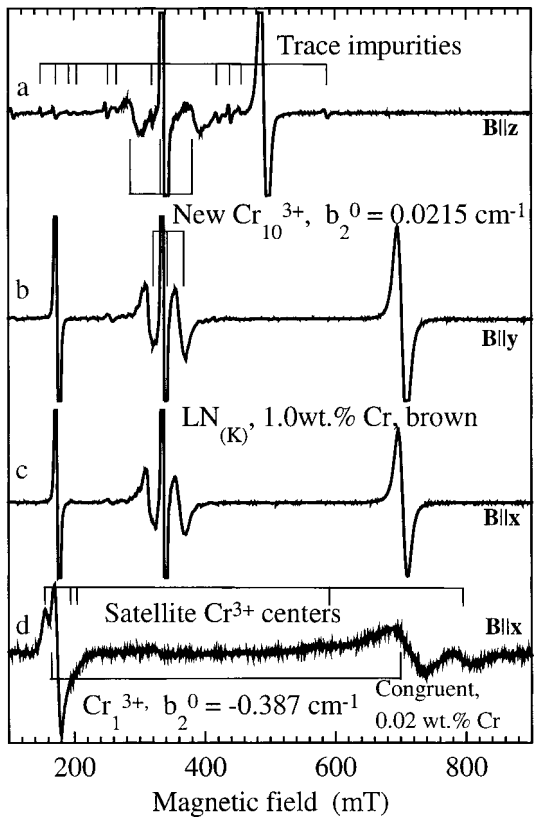

FIG. 3. The EPR spectra of Cr^{3+} in $LN_{(K)}$ (a)–(c) and congruent LN (d) for different orientations of the external magnetic field **B**. $T=5$ K, $\nu=9.4$ GHz.

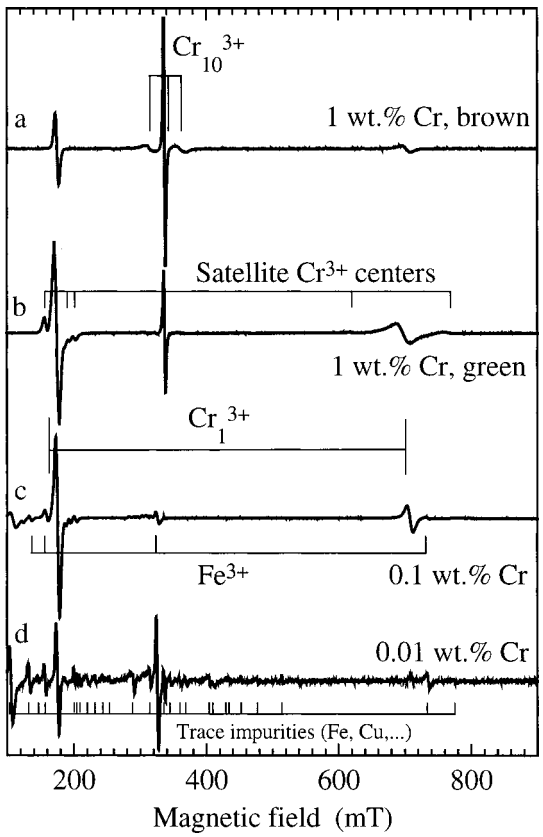

FIG. 4. The EPR spectra of $LN_{(K)}$ for different chromium concentrations. $T=5$ K, $\nu=9.4$ GHz, and $\mathbf{B}\|\mathbf{x}$.

tion. The observed colors of the samples reflect the redistribution of the optical absorption. To check on the appearance of a band near 500–550 nm in the $LN_{(K)}$-brown sample we supposed that the band at 660 nm can serve as the reference band for a characterization of the Cr^{3+}_{1-9} concentration: all these centers have similar crystal-field parameters, and no other centers have been found in congruent and $LN_{(K)}$ crystals doped with a low Cr concentration.

If the absorption coefficients at 660 nm, $\alpha_i(660)$, are proportional to the center concentrations, we can eliminate contributions of Cr^{3+}_{1-9} to the absorption coefficient of $LN_{(K)}$ crystals by subtraction of the correspondingly reduced absorption of congruent crystals. Following this, for $LN_{(K)}$-green and $LN_{(K)}$-brown we obtained curves *f* and *g* in Fig. 2. They obviously have the same band, with a maximum at 530 nm, and probably additional bands at 320–360 nm. The concentration of the centres responsible for the absorption at 530 nm in the $LN_{(K)}$-brown sample is several times higher than in the $LN_{(K)}$-green sample. The band at 530 nm can be attributed to (a) other Cr^{3+} centers or Cr ions of different charge states; (b) some other defects created during the growth process; and (c) a noncontrolled impurity, which may enter the crystal together with Cr. To determine definitely the origin of the new optical band and the structure of centers responsible for it, we carried out EPR and ENDOR studies of all Cr-doped samples.

III. EPR STUDY

An investigation of Cr^{3+} centers with electron spin $S=\frac{3}{2}$ in LN has a long history (see Ref. 20, and references in it). However, the only centers with zero-field splitting $\Delta \approx 0.8\,\mathrm{cm}^{-1}$ were observed in conventional LN:Cr crystals. Typical EPR spectra of the centers are given in Fig. 3(d). These centers are usually present in all our crystals doped with Cr. In a crystal grown with 1 wt % of Cr added to the $LN_{(K)}$ melt, a group of three EPR lines with a splitting twenty times smaller was registered [Figs. 3(a)–3(c)]. The observed ratio of integral intensities of the new and old ones (i.e., the ratio of concentrations of corresponding centers) was about 0.1–0.2 in $LN_{(K)}$-green and 1–1.2 in $LN_{(K)}$-brown [Figs. 4(a) and 4(b)]. To make a correct interpretation and identification of these lines we have to carry out a detailed study of their characteristics, since often even non-controlled impurities (Fe, Cu, Co, etc.) can be also seen due to tremendous narrowing of EPR lines in Li rich LN crystals.[22,24]

The lines belong to approximately axial defects, since their gravity centers have no angular dependence at the rotation of magnetic field in the **xy** crystallographic plane (Fig. 5). At an arbitrary orientation of the magnetic field, this group consists of three clearly distinguishable lines (fine structure). At some orientation of the magnetic field an additional badly resolved structure was also observed. Since the number of allowed EPR transitions is equal to $2S$, it would be natural to associate the visible fine triplet with the center with $S=\frac{3}{2}$. However, since the observed central line was always much narrower than the two others, a hypothesis about the existence of additional very broad lines with rather low peak-to-peak intensities ($S=\frac{5}{2}$ or even $S=\frac{7}{2}$) should be also considered.

To describe the observed spectra the following spin

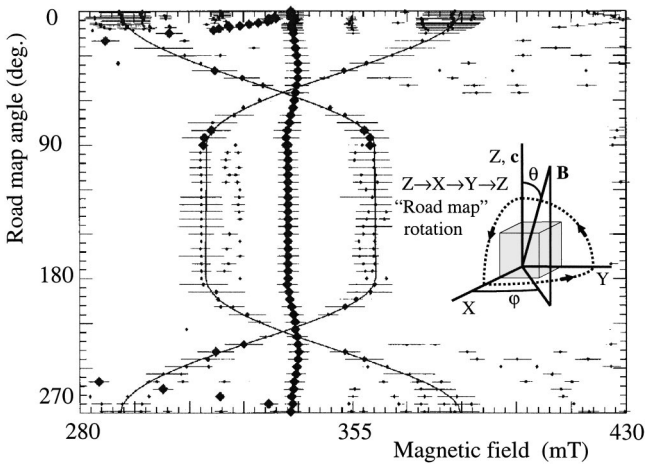

FIG. 5. Angular dependence (road map) of the EPR spectra of $LN_{(K)}$ with 1 wt. % of Cr. The error bars and the symbol sizes reflect the widths of the EPR lines, and the symbol sizes their intensities.

Hamiltonian with the axial symmetry was used:

$$H_{\mathrm{EPR}}=\beta\mathbf{BgS}+b_2^0\underline{O}_2^0. \tag{1}$$

Here β is the Bohr magneton, **B** is the vector of the static magnetic field, **g** is the g tensor, **S** is the total electron spin of paramagnetic center, b_2^0 is the parameter of the axial crystal field, and $\underline{O}_2^0=O_2^0/3$ is irreducible tensor operator of electron spin, which is defined in Ref. 25.

The best fitting of the angular dependencies of the gravity centers for all lines was obtained at $S=\frac{3}{2}$ and $g=1.995\pm0.005$, and $|b_2^0|=0.0215\pm0.001\ \mathrm{cm}^{-1}$ (zero-field splitting $0.043\ \mathrm{cm}^{-1}$; Fig. 5). It is also possible to fit the sidelines with $S=\frac{5}{2}$ or $\frac{7}{2}$; however, in these cases the calculated positions of the central line are out of the error bars. We label the center as Cr_{10}^{3+} with $S=\frac{3}{2}$, and the evidence of the assignment will be provided step by step.

One of the features of nonstoichiometric LN:Cr crystals is the presence of satellite centers consisting of paramagnetic impurity and intrinsic defects[20] [their lines are indicated in Fig. 3(d)]. In $LN_{(K)}$-green these satellite lines around lines of the old Cr^{3+} center are of very low intensities; however, they are still visible [Fig. 4(b)]; in $LN_{(K)}$-brown they are practically absent [Fig. 4(a)]. Therefore, we can conclude that the concentration of nonstoichiometric defects is rather low in $LN_{(K)}$-green and is extremely low in $LN_{(K)}$-brown, and that the inhomogeneity of crystal composition correlates with Cr_{10}^{3+} contents.

Another parameter, useful for the characterization of the degree of crystal imperfection, is the width of EPR lines (Table I). In such a ROC, like $LN_{(K)}$ with 0.01 wt % Cr, the main mechanism of line broadening is unresolved hyperfine structure. Therefore, the linewidths here are comparatively small, nearly equal for all transitions, and have a very weak dependence on the magnetic-field orientation. Intrinsic and extrinsic defects cause random distributions of the components of the crystal fields. If the line positions depend linearly on crystal-field parameters (like $\pm3/2\leftrightarrow\pm1/2$ transitions), this leads to an essential line broadening. If the crystal field produces only a second-order shift of the resonance line (the central $\frac{1}{2}\leftrightarrow-\frac{1}{2}$ transition), a moderate broadening and asymmetry of this line take place. A high concentration of intrinsic defects in Li-deficient congruent LN induces an increase of up to twice the linewidth for the central transition of Cr_1^{3+}, and one of up to ten times for $\pm3/2\leftrightarrow\pm1/2$ transitions. The EPR lines at $\mathbf{B}\perp\mathbf{z}$ are usually 1.6–2 times broader than at $\mathbf{B}\|\mathbf{z}$. This means that a random distribution of low-symmetry components $(b_2^1,c_2^1,b_2^2,c_2^2)$ makes the dominant contribution to the line width.

The linewidths of Cr_1^{3+} centers in both $LN_{(K)}$-green and $LN_{(K)}$-brown are much smaller then those in congruent LN; however, they are a little larger than in a ROC. This is in an agreement with the above conclusion made about the low concentration of intrinsic defects in $LN_{(K)}$. The linewidths of Cr_{10}^{3+}, and their dependence on the orientation of the magnetic field, are quite different from these for Cr_1^{3+} in a congruent crystal. The central EPR line of Cr_{10}^{3+} is narrower (2 mT only); it has no visible asymmetry, and a very weak angular dependence of the linewidth. The lines of $\pm3/2\leftrightarrow\pm1/2$ transitions at $\mathbf{B}\perp\mathbf{z}$ are 1.5–1.6 times narrower than that at $\mathbf{B}\|\mathbf{z}$, and 10–5 times broader than the central line.

To estimate a possible contribution of spin-lattice relaxation to line broadening, the dependence of the EPR spectra on the microwave power was measured. All of the lines of both Cr_1^{3+} and Cr_{10}^{3+} centers have partly different but similar dependencies; however, the corresponding relaxation rates are too slow to give an essential addition to the linewidth for any transition. The bell-like dependencies of line intensities on microwave power help us to find optimal conditions for ENDOR investigations. Since the central transition is less

TABLE I. Peak-to-peak linewidths of different transitions for chromium centers in LN (in mT).

		B$\|$**z**		**B**$\|$**x**	
Center	Crystal	$1/2\leftrightarrow-1/2$	$\pm3/2\leftrightarrow\pm1/2$	$1/2\leftrightarrow-1/2$	$\pm3/2\leftrightarrow\pm1/2$
Cr_1^{3+}	Congruent	6	32–36	10.5	50–60
	$LN_{(K)}$-green	3.5	15	5–5.5	15–17
	$LN_{(K)}$-brown	3.3	12–14	5	14–17
	$LN_{(K)}$, (ROC) 0.01 wt % Cr	3.0	4–6	4.3	4–6
Cr_{10}^{3+}	$LN_{(K)}$-green	2.0	18–20	2.7	14–16
	$LN_{(K)}$-brown	2.0	18–20	2.6	14

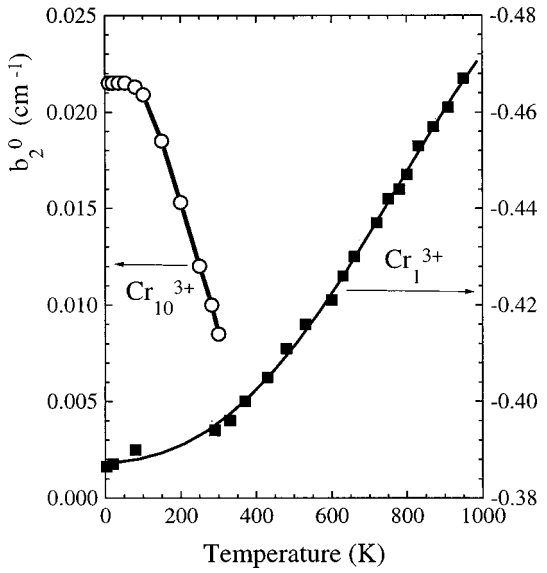

FIG. 6. Temperature dependence of the axial crystal-field parameter b_2^0 for Cr_1^{3+} and Cr_{10}^{3+}.

affected by crystal-field variations, the unresolved hyperfine interactions have to be responsible for this line broadening.

To find the origin of the line broadening and a reason for the visible deviation of the observed ratio of peak-to-peak intensities from the expected for $S=\frac{3}{2}$ ratio 3:4:3, a simulation of EPR spectra with a random distribution of crystal fields was made for the magnetic-field orientation $\mathbf{B}\|\mathbf{x}$, where the lines of Cr_1^{3+} and Cr_{10}^{3+} centers do not overlap. A good agreement of experimental and simulated spectra was obtained, supposing that a random distribution of the axial crystal field gives the dominant contribution, and that the width of this distribution Δb_2^0 is about 0.006 cm^{-1}. At the same time the values of Δb_2^0 are comparatively too small to produce a second-order shift of the central transition line and to cause its broadening or asymmetry. The larger linewidth of the $\pm 3/2 \leftrightarrow \pm 1/2$ transitions at $\mathbf{B}\|\mathbf{z}$ than at $\mathbf{B}\perp\mathbf{z}$ also becomes understandable, if we take into account their different dependences on b_2^0. The positions of these lines derived on the basis of Eq. (1) are given by expressions $g\beta B \pm 2b_2^0$ and $g\beta B \pm b_2^0$ at $\mathbf{B}\|\mathbf{z}$ and $\mathbf{B}\perp\mathbf{z}$, respectively. Since we found that $LN_{(K)}$-brown has an extremely low concentration of intrinsic defects, some extrinsic defects have to be the source of the random distortions of the crystal fields.

The temperature dependence of the axial crystal-field parameters for Cr_1^{3+} and Cr_{10}^{3+} centers has an opposite behavior. An absolute value of b_2^0 increases from 0.386 cm^{-1} at 4.2 K to 0.41 cm^{-1} at room temperature, and is even greater at high temperature,[26] whereas the line splitting for the new center goes to zero when temperature T rises, and practically disappears above room temperature (Fig. 6). In ferroelectric crystals the temperature dependence of spin Hamiltonian parameters can often be caused by a lattice transformation due to the phase transition. LN has such a transition from a ferroelectric $R3c$ phase to a paraelectric $R\bar{3}c$ phase at $T \approx 1540$ K. The observed smooth dependence $b_2^0(T)$ for Cr_1^{3+} can be caused by this transition.[27] However, in the temperature range between 4.2 and 400 K there are practically no changes of the positions of lattice ions; therefore, a disappearance of an axial crystal field for Cr_{10}^{3+} should be due to some other reason, for instance, to the ion movements in the nearest surrounding of the Cr impurity.

IV. ENDOR

The goal of our ENDOR study was to find the answers to several typical key questions: Are the EPR lines related to Cr ions or to some noncontrolled impurities like, for example, iron? What nuclei are present in the nearest surroundings of the centers? What kind of impurity ions or intrinsic defects serve as a charge compensator of the centers? What is similar and what is different in comparison with previously reported data about chromium centers?

Since at $\mathbf{B}\|\mathbf{z}$ the EPR lines of Cr_1^{3+} and Cr_{10}^{3+} centers overlap, the main measurements were carried out at $\mathbf{B}\perp\mathbf{z}$ to avoid ambiguity with the spectrum interpretation. The best ratio of the ENDOR signal to noise was found at temperatures of 4.2–5 K for the central EPR transition.

ENDOR frequencies are described by the addition of the spin Hamiltonian for the ith nucleus to the H_{EPR}:

$$H_i = -g_n^i \beta_n \mathbf{B}\mathbf{I}^i + \mathbf{S}\mathbf{A}^i\mathbf{I}^i + \mathbf{I}^i\mathbf{Q}^i\mathbf{I}^i. \tag{2}$$

Here β_n is the nuclear magneton, g_n is the nuclear g factor, and $\mathbf{A}$ and $\mathbf{Q}$ are tensors of the hyperfine and quadrupole interactions (relations between the Cartesian A_{pq}, Q_{pq} and irreducible A_2^q, Q_2^q components of second rank tensors were given in Ref. 23. Roughly the ENDOR line positions can be estimated as

$$\nu_M(i) = \nu_i + MA^i + Q^i m^i. \tag{3}$$

M and m^i are projections of electron and nuclear spins on corresponding quantization axis, and ν_i is the Larmour frequency of the ith nucleus. Explicit expressions for A^i and Q^i can be found, for instance, in Refs. 28–30. More precisely the ENDOR frequencies can be obtained by numerical diagonalization of

$$H = H_{\mathrm{EPR}} + \Sigma_i H_i. \tag{4}$$

We mainly used the following approach. At the first step, by numerical diagonalization, the energy levels E_M and wave functions $\langle M|$ of H_{EPR} were found, and matrix elements of electron spin $\langle M|\mathbf{S}|M'\rangle$ were calculated for all M and M'. Then, for each electron-spin state M, the matrices of effective nuclear spin-Hamiltonians H_i^M were built:

$$H_i^M = \langle M|H_i|M\rangle + \Sigma_{M'\neq M}\langle M|H_i|M'\rangle \times \langle M'|H_i M\rangle (E_M - E_{M'})^{-1}. \tag{5}$$

Finally, again the numerical diagonalization of H_i^N was used to calculate the nuclear sublevel energies, ENDOR frequencies, and relative probabilities of nuclear transitions.

The tensor of the interaction of a surrounding nucleus with the paramagnetic defect in the $\mathbf{C}_3$ position has $\mathbf{C}_3$ symmetry, if both are located on the crystal $\mathbf{z}$ axis, and $\mathbf{C}_1$ symmetry in all other cases (local symmetry of the nucleus). In the $R3c$ lattice each nucleus of the surrounding $\mathbf{C}_3$ center (except for the nucleus on the center axis) has two additional magnetically nonequivalent partners, which can be transformed into one another by a rotation around the $\mathbf{z}$ axis by

120° and 240°. These three nuclei are characterized by the same set of hyperfine and quadrupole parameters (a shell of electrically equivalent nuclei). If L and R partners[23] are not distinguishable by EPR (the case of axial Cr^{3+} centers), the ENDOR spectrum has a contribution of both centers. All parameters of the nuclear spin Hamiltonians for L and R centers have the same absolute values, but $A_{xy}(L)=-A_{xy}(R)$, $A_{zx}(L)=-A_{zx}(R)$, $Q_{xy}(L)=-Q_{xy}(R)$, $Q_{zx}(L)=-Q_{zx}(R)$ for tensors in Cartesian notations. In this situation each nuclear shell consists of six nuclei in the general case (this can reveal itself in an additional splitting of ENDOR lines with specific ''mirror'' angular dependencies). Therefore, at the arbitrary orientations of the magnetic field each low-symmetry shell of nuclei can produce $6\times(2S+1)\times 2I$ ENDOR lines.

If distances between paramagnetic defect and surrounding nuclei of the same type coincide, the parameters of the corresponding interactions can be nearly equal, which leads to nonresolved ENDOR lines. Any distortion preserving the center symmetry, for example, the shift of impurity ion along the **z** axis, can transform a part of these accidentally degenerated nuclear shells into independent shells with different parameters. The systematic presence of a foreign ion or regular ion vacancy on the z axis does not change the $\mathbf{C}_3$ symmetry of the axial center; however, it removes the accidental degeneration of nuclear shells. The same defect in one of low-symmetry shells of the nearest surrounding paramagnetic impurity leads to (a) the electrical nonequivalence of the two other ions of this shell, (b) the nonequivalence of all three ions of the neighbor shells, and (c) a lowering of local symmetry to $\mathbf{C}_1$ for nuclei at $\mathbf{C}_3$ sites. Consequently, a duplication [case (a)] and a triplication [cases (b) and (c)] of corresponding branches should be observed. For instance, the presence of an additional interstitial ion in the vicinity of $Me^{3+}_{Nb^{5+}}$ triples the lines of all Li and Nb shells. Naturally, the values of possible distortions (and correspondingly, the splitting of the ENDOR frequencies) become smaller with the increase of distances between the interstitial ion and investigated nuclei.

The glide mirror plane is an element of crystal symmetry, which transforms an L center to an R center. However, each of these $\mathbf{C}_3$ centers has no mirror plane symmetry. Therefore, for some shells their six nuclei are generally nonequivalent, although they are located at the same distance from the impurity ion (for instance, six Nb nuclei in the **xy** plane around the Me_{Nb} center). The knowledge of these features helps to decipher the ENDOR spectra, and to determine the center structures.

A. ENDOR of chromium nucleus

Typical triplet lines with an isotropic hyperfine interaction (HFI) about 50 MHz are the strongest lines in ENDOR spectra of both new and old centers. They definitely belong to ^{53}Cr nuclei (nuclear spin $I=\frac{3}{2}$, natural abundance $N_a=9.5\%$). The known noncontrolled impurities (C, Cu, Fe, V, etc.) can be excluded, because they have nuclei with other I or with very small abundance. The determined parameters of quadrupole interaction with their own nuclei are equal to 0.14 for Cr^{3+}_{10} and -0.32 MHz for Cr^{3+}_{1}. This means that a gradient of electric fields at the point where the nucleus of Cr^{3+}_{10} is located is essentially smaller than on the Li site, occupied with the chromium ion of the Cr^{3+}_{1} center. This correlates with the small value of the axial crystal-field parameter for Cr^{3+}_{10} centers.

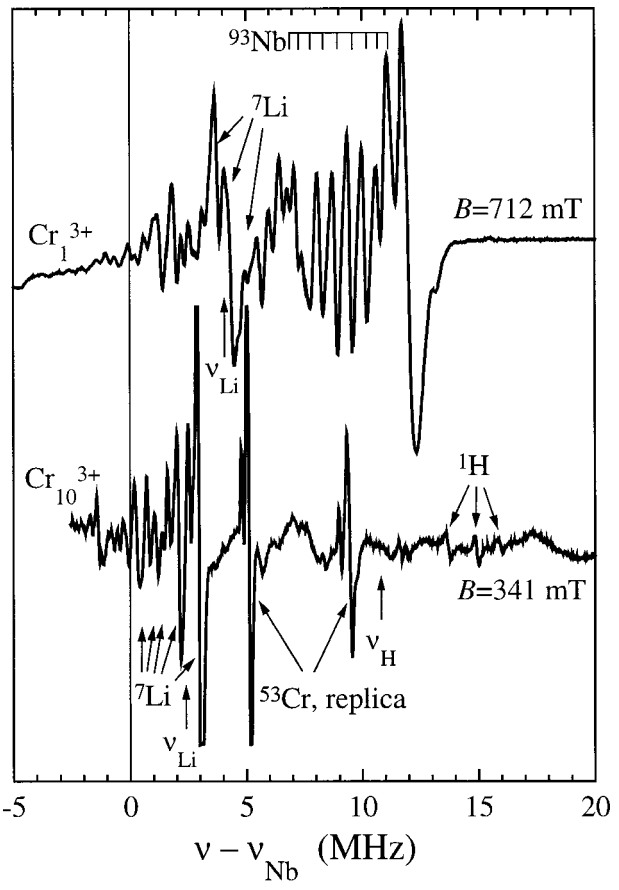

FIG. 7. The ENDOR spectra of Cr^{3+}_{1} (high-field EPR transition) and Cr^{3+}_{10} (central EPR transition) at $\mathbf{B}\|\mathbf{x}$, $T=5$ K. To facilitate a comparison of the spectra, they were shifted to the ^{93}Nb Larmour frequencies.

The HFI with its own nucleus for Cr^{3+}_{10} has weak anisotropies. $A_{xx}=A_{yy}=51.1$ MHz and $A_{zz}=50.7$ MHz. Some replicas of the main ^{53}Cr signals were also registered at the frequencies $\nu_M(\mathrm{Cr})/2$, $\nu_M(\mathrm{Cr})/3$, $\nu_M(\mathrm{Cr})/4$ and $\nu_M(\mathrm{Cr})/5$ (Fig. 7).

B. ENDOR of surrounding nuclei

ENDOR spectra of Cr^{3+}_{1} and Cr^{3+}_{10} (Fig. 7) are completely different. In the spectra of Cr^{3+}_{1}, multiplets of nine lines of ^{93}Nb are clearly distinguishable. These Nb nuclei have the strongest HFI, since they are located in the nearest cation surroundings of the chromium ion substituted Li[31]. No such multiplets were found for Cr^{3+}_{10} despite variations of measurement conditions (microwave and radio-frequency powers, change of magnetic field within the EPR line, temperature, etc.).

The measured angular dependencies of the ENDOR spectra of Cr^{3+}_{10} for the central $\frac{1}{2}\leftrightarrow-\frac{1}{2}$ EPR transition are presented in Figs. 8 and 9. All of the observed lines have the angular repetitions, which reflect the $R3c$ symmetry of LN; however, they do not have any resolved quadrupole splitting.

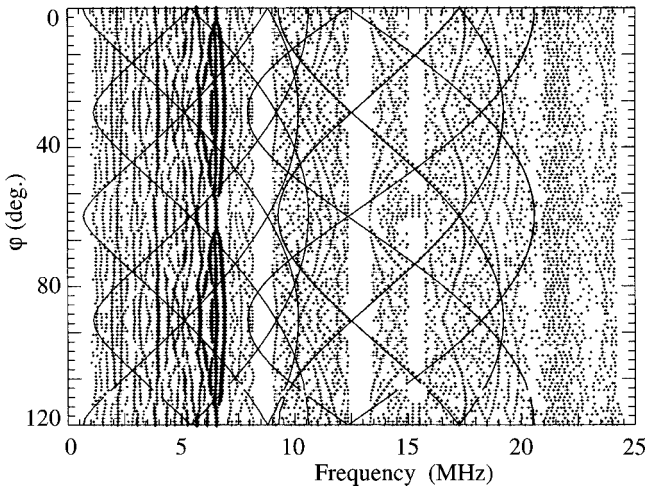

FIG. 8. Measured angular dependencies of the ENDOR spectra of Cr_{10}^{3+} (symbols) and calculated dependencies (lines) for one of the ^{7}Li nuclei (No. 2b in Table II) in the **xy** plane. $T=5$ K and $B=341$ mT.

The lines without angular dependence (except for the lines of ^{53}Cr) were not detected. The nuclear transitions for all four values of the electron-spin projection M ($\pm 3/2$ and $\pm 1/2$) were found (probably, due to overlapping of $\pm\frac{3}{2}\leftrightarrow\pm\frac{1}{2}$ EPR transitions with the line of the $\frac{1}{2}\leftrightarrow-\frac{1}{2}$ transition).

The lines of the first group are centered at Larmour frequency of ^{7}Li nuclei $\nu_{\mathrm{Li}}\approx 5.8$ MHz. At least six nuclei with different HFI have been found. Their angular dependencies have the extrema at azimuthal angles φ about 30°, 60°, and 90°. They were successfully fitted with two parameters only (Table II). It is natural to associate these lines with the ^{7}Li nuclei. Since the structural vacancies are located at the same azimuthal directions as regular Li sites, it is impossible at present to distinguish definitely the positions of Li nuclei responsible for the observed lines. Some of the lines may belong to additional Li^+ ions in the structural vacancies, Li_v^+, the others to regular Li^+ ions in the nearest and next-nearest neighborhoods.

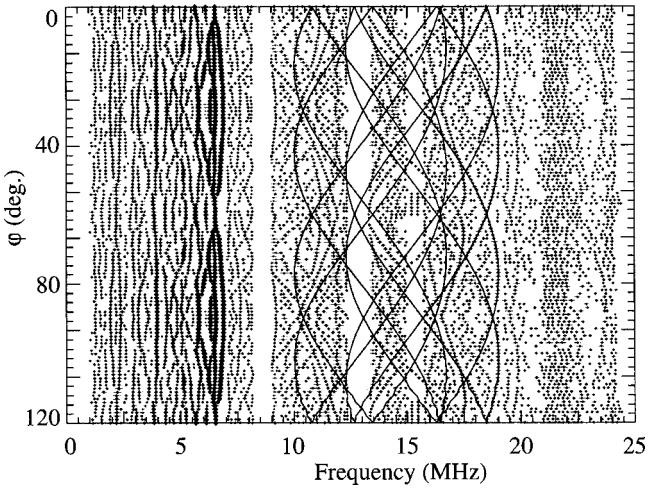

FIG. 9. Measured angular dependencies of the ENDOR spectra of Cr_{10}^{3+} (symbols) and calculated dependencies (lines) for one of the hydrogen nuclei (No. $h2$ in Table II). $T=5$ K and $B=341$ mT in the **xy** plane.

TABLE II. Parameters of hyperfine interactions (in MHz), which describe the measured angular dependencies of ENDOR lines for Cr_{10}^{3+} in $LN_{(K)}$ at the rotation of the magnetic field in the **xy** plane.

Nucleus	Position (shell) No.	A_{xx}	A_{yy}	A_{xy}
^{7}Li	1	?	?	?
^{7}Li	2a	−12.1	12.3	0
^{7}Li	2b	−9.95	9.05	0
^{7}Li	2c	−8.25	5.3	0
^{7}Li	3a	−2.65	5.05	0
^{7}Li	3b	−1.9	4.0	0
^{7}Li	3c	−0.9	2.4	0
^{1}H	$h1$	9.8	−2.1	±3.9
^{1}H	$h2$	7.8	−3.2	±3.9
^{1}H	$h3$	5.7	−3.3	±0.2

The lines of the second group have rather high frequencies about 10–20 MHz and the extrema of their angular dependencies occur at φ about 16°–17°. There are no regular lattice ions in these directions. If we suppose that these lines are related to the additional Li ions, the values of corresponding HFI parameters have to be about 20–25 MHz, which is in obvious contradiction with the measured width of EPR line for this center (2 mT). Since these lines are centered on the ^{1}H Larmour frequency ν_{H}, we fitted them as related to hydrogen nuclei and obtained a rather good agreement with the observed frequencies at reasonable values of parameters (see Table II). Part of the calculated angular dependencies is drawn in Figs. 8 and 9. If we suppose that the extrema of angular dependencies correspond to the directions from a chromium ion to the possible nucleus positions

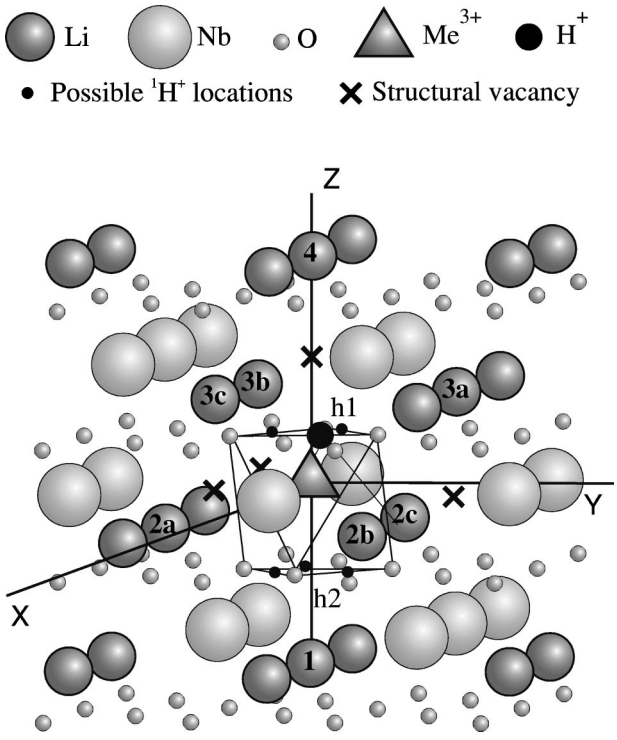

FIG. 10. Possible configurations of Cr^{3+} substituting for Nb, and charge-compensating defects.

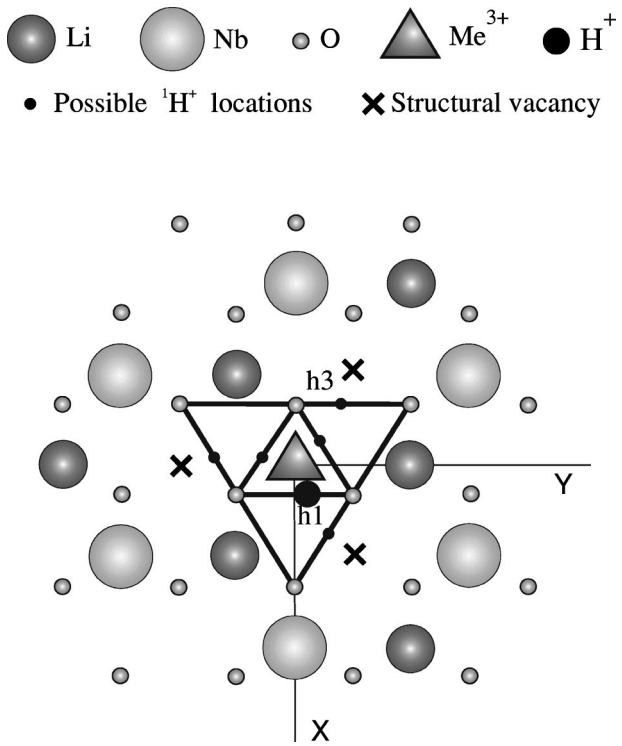

FIG. 11. Possible configurations of Cr^{3+} substituting for Nb, and charge-compensating defects. A projection on the **xy** plane is shown.

(which is valid for dipole-dipole interactions, though it is not obligatory in the general case), we have to conclude that $h1$ and $h2$ positions of $^1H^+$ are shifted from the center of the O-O bond on about one-eighth of its length. Since the parameters for $h3$ shell are smaller than those for $h1$ and $h2$, the distance to this position should be greater. $^1H^+$ of the $h3$ shell is probably located on the next O-O bond (Figs. 10 and 11).

Each line with $A_{xx} \neq A_{yy}$ belongs to the nucleus, which is not located on the center axis. According to crystal symmetry a shell of such nuclei consists of three, six, or 12 electrically equivalent nuclei. An attempt to reconstruct an EPR line, supposing that each nucleus listed in Table II has two or more additional partners, fails: the calculated linewidth of the $\frac{1}{2} \leftrightarrow -\frac{1}{2}$ transition is greater than the observed one. Therefore we have to conclude that only part of the listed nuclei belongs to the one Cr_{10}^{3+} center. Being equivalent in the sense of EPR (nearly equal g and b_2^0 parameters), Cr_{10}^{3+} centers are not equivalent from the point of view of ENDOR. This means that, like in the case of Cr_{1-9}^{3+} centers, low crystal field Cr_{10}^{3+} creates a family of similar, but not identical, centers. The difference in crystal-field parameters of the Cr_{1-9}^{3+} centers, with a zero-field splitting about 0.8 cm^{-1} was so large that it was possible to resolve their lines even by EPR.[20] Centers with $b_2^0 \approx 0.0215\,cm^{-1}$ have a much smaller difference of the parameters (with a distribution of about 0.006 cm^{-1}; see Sec. III); therefore, they can be distinguishable only with the help of ENDOR.

The observed HFI for the nearest Li nuclei at a distance of 3 Å (8–12 MHz;; see Table II) strongly deviates from the calculated dipole-dipole interactions (about 1.1 MHz only; see Table III). For $^1H^+$ the estimated dipole-dipole values (9.5–2.8 MHz at the distances 2–3 Å) are close to the parameters of the observed HFI. Therefore, we can conclude that electronic density of the Cr_{10}^{3+} center is rather delocalized and anisotropic. The presence of H^+ in the chromium neighborhood would be very unlikely if Cr_{10}^{3+} substitutes for Li^+, or incorporates itself into the structural vacancy—in both these cases an additional negative charge is required for the compensation.

V. MODELS OF CHROMIUM CENTERS IN LITHIUM NIOBATE

Finally, we came to the conclusion that the following model is able to explain all experimental details of the Cr_{10}^{3+}

TABLE III. Nucleus positions and dipole-dipole interactions for the paramagnetic defect on the Nb site.

Nucleus	Sphere	Symmetry	Number of nuclei	Distance	Projection on the c axis	b_{dd}, MHz	α	β	Comment
Li	1	C_3	1	3.009	3.009	1.128	0	0	
Li	2	C_1	3	3.053	−0.70	1.084	30, 120, 270	−76.77	
Li	3	C_1	3	3.381	1.61	0.796	−30, 90, 210	61.53	
Li	4	C_3	1	3.922	3.922	0.510	0	0	
Li	5a,5b	C_1	3+3	5.963	−1.61	0.196	0, 60,...,300	59.69	[a]
Nb	1a	C_1	3	3.765	2.31	0.364	30, 150, 270	52.14	[b]
Nb	1b	C_1	3	3.765	−2.31	0.364	−30, 90, 210	−52.14	[b,a]
Nb	2a,2b	C_1	3+3	5.148	0	0.142	0, 60,...,300	90	
Nb	3a	C_1	3	5.494	4.62	0.117	−30, 90, 210	32.75	[b]
Nb	3b	C_1	3	5.494	−4.62	0.117	30, 150, 270	−32.75	[b,a]
Nb	4a	C_1	3	6.378	2.31	0.072	−30, 90, 210	68.76	[b]
Nb	4b	C_1	3	6.378	−2.31	0.072	30, 150, 270	−68.76	[b,a]
Nb	5	C_3	1	6.932	6.932	0.058	0	0	

[a]The nuclei of the sphere were not indicated previously (Ref. 30) because only the upper part of the crystal lattice was considered.

[b]The lines of a and b spheres of these nuclei are split, if the defect shifts off the normal lattice position.

center. Since the chromium ion has regular Li nuclei in the nearest neighborhood, it substitutes for Nb^{5+}. A lack of two positive charges cannot be locally compensated for by the nearest oxygen vacancy or by the nearest Nb_{Li}, since such defects should give a much greater low-symmetry perturbation of crystal field than the observed one. Since $^1H^+$ lines found in ENDOR spectra are characterized by rather strong HFI, the interstitial H^+ should be located in the vicinity of Cr, and provide the necessary charge compensation. Three previously equivalent Li nuclei of any shell become nonequivalent in the presence of even one $^1H^+$ (or it is the same: OH^-) in the neighborhood of the Cr ion. In a common case shell No. 2, for instance, splits into $2a$, $2b$, and $2c$ subshells, i.e., three nuclei have similar, but not identical, HFI parameters. The observed repetition of angular dependencies at 120° from the mirror plane at $\varphi = 30°$ (the **zy** plane) is a result of a superposition of many centers: each of them has low symmetry; however, a total picture reflects the crystal symmetry. A supposition that each nucleus listed in Table II has no partners allows one to overcome the above-indicated difficulty in EPR line reconstruction.

Based on the available data, we cannot exclude the presence of additional Li ions in structural vacancies Li_v^+, since nuclei in these and regular Li positions have similar angular dependencies in the **xy** plane. One can imagine several configurations with local or distant charge compensations, two Li_v^+, two H^+, one Li_v^+ and one H^+; one Li_v^+ or H^+ in the nearest neighborhood; and another Li^+, H^+ or Cr_{Li}^{3+} ion in one of the distant shells (the typical configurations for hydrogen ions are presented in Figs. 10 and 11). H^+ can be coupled with O^{2-} in the oxygen layers above or below Cr ions. The existence of several possible configurations easily explains the observed difference of linewidths for $\frac{1}{2} \leftrightarrow -\frac{1}{2}$ and $\pm\frac{3}{2} \leftrightarrow \pm\frac{1}{2}$ transitions. The near disappearance of the axial crystal-field parameter of Cr_{10}^{3+} at a temperature of about 400 K is probably related to the movement of H^+ around Cr.

The models of the old Cr_1^{3+} center and Cr_{10}^{3+} are completely different. In the first case Cr^{3+} substitutes for Li^+, and has an excess of positive charge, which can be compensated for by intrinsic defects, like Nb and Li vacancies.[20] In the second case the Cr^{3+} ion replaces Nb^{5+}, and is negatively charged relative to the regular lattice. Theoretically, some intrinsic nonstoichiometric defects, for example $Nb_{Li^+}^{5+}$ antisites, could serve as distant compensators for these centers. However, Cr_{10}^{3+} centers do not appear in congruent LN at a low chromium concentration (more exactly, they did not appear until [Cr] was less than the concentration of nonstoichiometric defects). The procedure for the growth of $LN_{(K)}$ crystals reduces the concentration of nonstoichiometric defects up to a very low level, and Cr_1^{3+} centers bind the rest of conventional intrinsic defects. This creates the conditions, when Cr, seeking a charge compensator, enters the crystals together with some of the available extrinsic defects—in our case with H^+.

VI. DISCUSSION

It is interesting to note one unexpected and amazing fact: the properties of congruent LN crystals heavily doped with such modifiers as Mg, Zn, or Ca, and codoped with the Cr in a rather low concentration, have many features similar (but not identical) to those reported here for regularly ordered LN with a high Cr content (about 1% in the melt).

The coloration of the LN:Mg:Cr crystal studied in Ref. 32 was rather inhomogeneous along the **z** axis: the upper and lower parts of the crystal boule were greenish and violet, with a continuous transition range between them. Green color for the samples with 2% and 4% of MgO, and brown color for the samples with 5.5% and 6% of MgO were reported in Ref. 33. The band at 530 nm with an absorption coefficient about 1 cm^{-1} at the maximum was extracted in Ref. 32; it is not so pronounced as in our Fig. 2(c), but the Cr concentration in the melt used for the growth of LN:Mg:Cr was smaller. The bands at 530 and 300 nm were explained as crystal fields transitions of Cr^{4+} (but not Cr^{3+}) ions.[32] The presence of H^+ in the Cr neighborhood was used for the interpretation of new band in the infrared absorption region at 3506 cm^{-1} as OH stretching vibration in Cr-OH-Mg complexes.[32] In Ref. 33 one of the OH^- bands was associated with the complex of $Cr_{Li^+}^{3+}$-OH^--$Mg_{Nb^{5+}}^{2+}$, but not with $Cr_{Nb^{5+}}^{3+}$.

In studies by EPR and ENDOR,[34,35] optically detected magnetic resonance,[36] and optical absorption and EPR investigations of LN:Mg:Cr[37–40] as well as LN:Zn:Cr[37] and LN:Ca:Cr,[41] Cr^{3+} center with very low crystal-field parameter b_2^0 was observed. Its EPR spectrum consisted of only one central line (the sidelines were not visible either due to overlapping with the central line or to very small intensities, or for both these reasons simultaneously). It was impossible to determine the value of b_2^0 directly; nevertheless, with the help of an indirect procedure it was roughly estimated[34] as $b_2^0 \leqslant 0.01\ cm^{-1}$. In contrast to Ref. 32, the additional optical absorption band at 530 was correlated to this nearly isotropic Cr^{3+} center with $g = 1.971$,[35,36] and no other ions, except Li and Nb, were found in the Cr surrounding by ENDOR measurements[34] of the same crystal. The observed HFI (about 1–2 MHz or less) were interpreted as close to classical point dipole-dipole interactions of Cr substituting for Nb and surrounding nuclei.[34] The authors concluded that Cr shifted by about 0.1 Å toward the center of octahedron. particle induced x-ray emissio (PIXE)/channeling data[42] supported Nb substitution in the LN:Mg:Cr, and the indicated shift value.

The similarity of these and some other properties of Li-rich and Mg-doped LN crystals (for example, the blueshift of the fundamental absorption edge) coexists at the same time with the opposite behavior of many other properties (linewidths of EPR, NMR,[22] and Raman scattering,[10] lattice constants,[43] etc). Crystals heavily doped with the above-mentioned modifiers obviously have a defect concentration much higher (but not lower), than conventional undoped materials. Since Mg^{2+} ions are not isocharged to Li^+ or Nb^{5+} ions, these extrinsic defects can serve as charge compensators for trivalent ions. For instance, a complex of $Me_{Nb^{5+}}^{3+}$-$2Mg_{Li^+}^{2+}$ is fully compensated for, and there is no necessity to involve other extrinsic defects for the charge compensation.

The superficial resemblance of LN:Mg:Cr, LN:Zn:Cr, and $LN_{(K)}$:Cr turns into a profound difference at close consider-

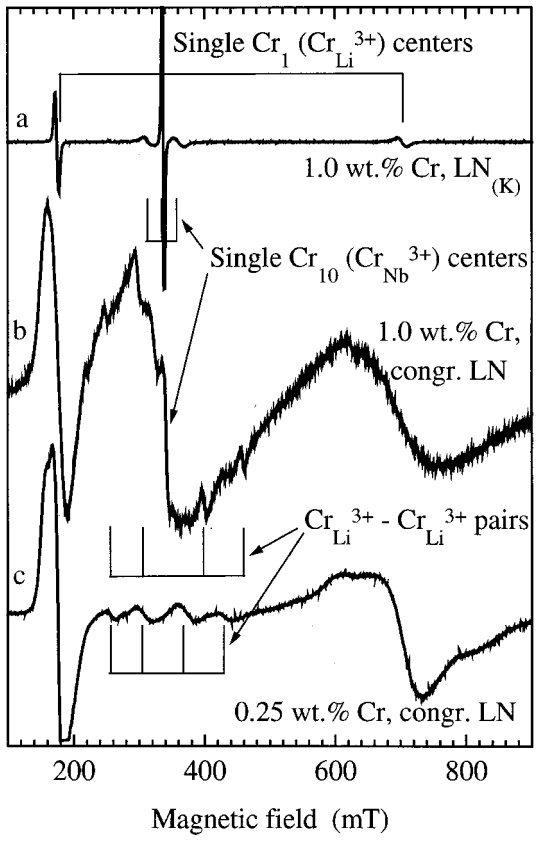

FIG. 12. Comparison of the EPR spectra of crystals highly doped with Cr:$LN_{(K)}$ and congruent LN. $\nu = 9.4$ GHz and $T = 5$ K, $\mathbf{B} \| \mathbf{x}$ [(a) and (b)]. **B** close to **x** (c).

ation. The Cr_{10}^{3+} center appears in $LN_{(K)}$ without the addition of modifiers, though only at a rather high (about 1 wt. %) concentration of Cr in the melt. The ratio of integral intensities of the EPR line for Cr_1^{3+} and Cr_{10}^{3+} centers in $LN_{(K)}$-green and $LN_{(K)}$-brown (Fig. 4) corresponds approximately to the ratio of intensities of optical-absorption bands at 660 and 530 nm (Fig. 2). Therefore, there is only the possibility to associate the band at 530 nm definitely with a transition of the Cr_{10}^{3+}(Nb) center, but not with the other Cr position or other charge states. The obtained value of the axial crystal-field parameter b_2^0 for this center is two times higher, and values of the HFI with the Li nuclei are up to eight times higher than those estimated for the Cr^{3+} center in LN:Mg.[34] The presence of H^+ in the neighborhood of the Cr_{10}^{3+} center leads to a splitting of Li shells into subshells of nonequivalent nuclei. ENDOR gives evidence of the mechanism of charge compensation by hydrogen ions. Moreover, Cr_{10}^{3+} is not a single center, but a family of the centers, which differ from each other in the location of H^+ in the Cr neighborhood. The coexistence of Cr_1^{3+} and Cr_{10}^{3+} takes place in $LN_{(K)}$; however, Cr_1^{3+} is not observed in the crystals heavily doped with Mg or Zn.

It seems there is a rather obvious necessity for a comparative investigation of impurity centers in both kinds of crystals (undoped and heavily doped with modifiers) by different complementary methods. Such a study is strongly desirable, and would be very useful for correct conclusions about the nature of intrinsic and extrinsic defects in LN.

The exchange-coupled pairs were observed by EPR in congruent crystals at comparatively low (about 0.1–0.25 wt % in the melt; Fig. 12) concentrations of Cr.[44–47] Since their lines are split at the deviation of the magnetic field **B** from the crystal **c** axis, these centers are nonaxial, low-symmetry complexes. It was found[44] that the main component of crystal field $b_2^0(S)$ for multiplets with total spin $S = 3$ is about 0.164 cm^{-1}. According to the theory of exchange pairs this value has to be close to $(b_{2,A}^0 + b_{2,B}^0)/5$, where $b_{2,A}^0$ and $b_{2,B}^0$ are axial crystal-field parameters of the first and second ions in the dimer. A dimer, consisting of $Cr_{Li^+}^{3+}$ with $b_{2,\mathrm{Li}}^0 = 0.387\,cm^{-1}$ and $Cr_{Nb^{5+}}^{3+}$ with $b_{2,\mathrm{Nb}}^0 = 0.0215\,cm^{-1}$, should have $b_2^0(3) = (0.387 + 0.0215)/5 = 0.082\,cm^{-1}$, whereas a dimer consisting of two $Cr_{Li^+}^{3+}$ should have $b_2^0(3) = 2 \times 0.387/5 = 0.155\,cm^{-1}$. The last value is very close to measured 0.164 cm^{-1}; therefore we can now state that the observed dimers are complexes of two $Cr_{Li^+}^{3+}$ (glued by one niobium vacancy[20]), but not $Cr_{Li^+}^{3+}$-$Cr_{Nb^{5+}}^{3+}$ pairs. The low symmetry of registered dimers is in agreement with the nonaxial location of two nearest Li sites, whereas the nearest Li and Nb sites are located on the **c** axis (see Fig. 10). It is rather unexpected, but there is a fact, that chromium ions do not create the local self-compensated pairs (at least such pairs were not registered by EPR). Instead of that $Cr_{Li^+}^{3+}$ and $Cr_{Nb^{5+}}^{3+}$ ions prefer to be isolated and to have different compensation mechanisms, even if they are both present in the crystal in nearly equal concentration.

The comparison of the EPR spectra of congruent crystals doped with 0.25 and 1 wt % of Cr and $LN_{(K)}$ with 1 wt % of Cr (Fig. 12) shows that a sharp line with $g \approx 2$ does not present in congruent crystals at low Cr concentration; however, it appears in highly doped samples. If we suppose that the $\pm\frac{3}{2} \leftrightarrow \pm\frac{1}{2}$ transitions are not resolved due to the overlapping with the broad lines of exchange-coupled pairs, then we should also conclude about the presence of Cr_{10} centers in conventional congruent LN with a high Cr content. This means that there is a threshold concentration $[\mathrm{Cr}]_{\mathrm{thresh}}$ at which intrinsic defects are not able more to compensate completely for all $Cr_{Li^+}^{3+}$. If $[\mathrm{Cr}] > [\mathrm{Cr}]_{\mathrm{thresh}}$, chromium ions start to replace Nb ions in addition to Li ions. In the last case a part of Cr ions plays the role of a modifier (like Mg or Ca) for the other part. For $LN_{(K)}$ crystals having a very low content of intrinsic defects, this $[\mathrm{Cr}]_{\mathrm{thresh}}$ is much lower than for the congruent ones.

VII. CONCLUSION

Detailed investigations of EPR, ENDOR, and optical-absorption spectra allowed us to clarify the structure of the family of Cr^{3+} paramagnetic centers with $g = 1.995 \pm 0.005$, $|b_2^0| \approx 0.0215 \pm 0.001\,cm^{-1}$ and an optical band at 530 nm. Since ENDOR study has shown that electrons of Cr_{10}^{3+} center have a strong HFI with the nearest Li nuclei, the conclusion was made about Cr substitution for Nb (in contrast to the Cr_1^{3+} center, where Cr has a strong HFI with the Nb nuclei and replaces Li). Several ENDOR lines, which belong to $^1H^+$, were detected, and this sheds light on one of the mechanisms of local charge compensation of the Cr_{Nb} centers. The second possible mechanism is charge compensation

by additional Li ions in structural vacancies Li_v^+. The common feature of the found family is the Cr substitution for Nb. The various members of the family have different locations of interstitial H^+ or Li_v^+. The presence of a charge compensator in the nearest neighborhood causes lattice distortion, and leads to the distribution of crystal-field parameters, which reveals itself in the observed broadening and nonresolved structure of the $\pm\frac{3}{2}\leftrightarrow\pm\frac{1}{2}$ EPR transitions. The HFI parameters with several surrounding nuclei were determined, and a splitting of shells of equivalent nuclei into subshells was found. The observed HFI is of both Cr_{Li} and Cr_{Nb} centers are much stronger than dipole-dipole interactions, i.e., there are high electron densities on the nearest nuclei.

The mechanism of charge compensation by interstitial H^+ and/or by Li_v^+ can be realized not only for Cr^{3+} but for the other impurities, which also have a tendency to replace Nb. It is expected that this mechanism certainly works in crystals with a considerably decreased concentration of intrinsic defects (like $LN_{(K)}$ or VTE LN). Since an additional OH^- band in the infrared-absorption region at 3506 cm^{-1} appears in LN:Mg:Cr, the compensation of Me_{Nb} by H^+ probably also works in crystals highly doped with divalent and trivalent elements (like Mg, Zn, Ca, Sc, etc).

The Li replacing impurities, Me_{Li} (Cr is just an example) may have a threshold concentration, when they start to replace Nb ions. The conditions of the appearance of Me_{Nb} will, however, vary from impurity to impurity, and correspond to a special concentration balance between the considered kinds of impurity and intrinsic defects.

Our results show a strong interrelation between subsystems of intrinsic and extrinsic defects. If we come nearer to materials having vanishingly small numbers of intrinsic defects, then not only quantitative, but also qualitative changes of crystal characteristics are observed. The use of a ROC for the investigation of extrinsic defects is a very helpful and efficient method, due to its tremendous resolution enhancement of its spectra. The appearance of interesting features in the nearly perfect material illustrates the possibility to tailor LN properties by variations of concentrations of both intrinsic defects and impurities. The accumulated knowledge about charge compensation mechanism of different nonisovalent impurities allows one in the future to proceed to a more efficient intentional engineering of LN crystals with the required characteristics, instead of previous numerous attempts at blind manipulation with dopants, growth conditions, post-growth reduction, or oxidation treatment.

ACKNOWLEDGMENTS

Our sincere and deep gratitude goes to O. Schirmer for the opportunity to perform this work, for his qualified help, and permanent altruistic interest to this topic. We are very grateful to E. Kokanyan for the skillful growth of numerous, good quality Li-rich and $LN_{(K)}$ crystals, E. Bondarenko for the creative attitude to crystal preparation, J. Selinger for help with taking digital photos, and W. Kozlowski for the technical assistance. Partial support from INTAS-96 (Project No. 0599), Sonderforschungsbereich-225, and BMBF (Germany, Project No. UKR-034-96) is gratefully appreciated.

*E-mail address: vgrachev@uos.de

†E-mail address: gmalovic@uos.de

[1] A. Räuber, in *Current Topics in Material Sciences*, edited by E. Kaldis (North-Holland, Amsterdam, 1978), Vol. 1, p. 481.

[2] R. S. Weis and T. K. Gaylord, Appl. Phys. A: Solids Surf. **37**, 191 (1985).

[3] G. I. Malovichko, V. G. Grachev, V. T. Gabrielyan, and E. P. Kokanyan, Fiz. Tverd. Tela (Leningrad) **28**, 2593 (1986) [Sov. Phys. Solid State **28**, 1453 (1986)].

[4] N. Iyi, K. Kitamura, F. Izumi, J. K. Yamamoto, T. Hayasgi, H. Asano, and S. Kimura, J. Solid State Chem. **101**, 340 (1992).

[5] D. H. Jundt, M. M. Fejer, and R. L. Byer, IEEE J. Quantum Electron. **26**, 135 (1990).

[6] P. F. Bordui, R. G. Norwood, C. D. Bird, and G. D. Calvert, J. Cryst. Growth **113**, 61 (1991).

[7] C. Fischer, S. Kapphan, Xi-Qi Feng, and Ning Cheng, Radiat. Eff. Defects Solids **135**, 199 (1995).

[8] G. Malovichko, V. Grachev, L. Yurchenko, V. Proshko, and E. Kokanyan, in *Defects in Insulating Materials*, edited by O. Kanert and J.-M. Spaeth (World Scientific, Singapore, 1993), p. 1124.

[9] G. I. Malovichko, V. G. Grachev, L. P. Yurchenko, V. Y. Proshko, E. P. Kokanyan, and V. T. Gabrielyan, Phys. Status Solidi A **133**, K29 (1992).

[10] G. I. Malovichko, V. G. Grachev, E. P. Kokanyan, O. F. Schirmer, K. Betzler, B. Gather, F. Jermann, S. Klauer, U. Schlarb, M. Wöhlecke, Appl. Phys. A: Solids Surf. **56**, 163 (1993).

[11] G. I. Malovichko, V. G. Grachev, O. F. Schirmer, and B. Faust, J. Phys.: Condens. Matter **5**, 3971 (1993).

[12] A. Kling, J. G. Marques, J. G. Correia, M. F. da Silva, E. Dieguez, F. Agullo-Lopez, and J. C. Soares, Nucl. Instrum. Methods Phys. Res. B **113**, 293 (1996).

[13] V. Bermudez, P. S. Dutta, M. D. Serrano, and E. Dieguez, J. Phys.: Condens. Matter **9**, 6097 (1997).

[14] K. Kitamura, Y. Furukawa, and N. Iyil, Ferroelectrics **202**, 21 (1997).

[15] K. Polgar, A. Peter, L. Kovacs, G. Corradi, and Zs. Szaller, J. Cryst. Growth **177**, 211 (1997).

[16] A. de Bernabe, C. Prieto, and A. de Andres, J. Appl. Phys. **79**, 143 (1995).

[17] M. H. Garret, I. Mnushkina, Y. Furukawa, K. Kitamura, L. E. Halliburton, N. C. Giles, and S. D. Setzler, in *Proceedings of 1997 Topical Meeting on Photorefractive Materials, Effects and Devices, June 11–13, 1997* (Chiba, Japan, 1997), p. 295.

[18] F. Abdi, M. Aillerie, P. Bourson, M. D. Fontana, and K. Polgar, J. Appl. Phys. **84**, 2251 (1998).

[19] Y. N. Choi, S. H. Choh, I. W. Park, E. K. Koh, and S. S. Kim, J. Korean Phys. Soc. **32**, S643 (1998).

[20] G. Malovichko, V. Grachev, E. Kokanyan, and O. Schirmer, Phys. Rev. B **59**, 9113 (1999).

[21] G. I. Malovichko, V. G. Grachev, and O. F. Schirmer, Solid State Commun. **89**, 195 (1994).

[22] G. Malovichko, V. Grachev, and O. Schirmer, Appl. Phys. B: Lasers Opt. **68**, 785 (1999).

[23] V. Grachev, 1992–1999. All details and the light version to

download can be found on the home page http://www.physik.uni-osnabrueck.de/resonanz/Grachev.

[24] G. Malovichko, *OSA Trends in Optics and Photonics, Vol. 27. Advances in Photorefractive Materials, Effects and Devices*, edited by P. E. Andersen, P. M. Johansen, H. C. Pedersen, P. M. Petersen, and M. Saffman (Optical Society of American, Washington, D.C. 1999), pp. 59–66.

[25] S. A. Altshuler and B. M. Kozirev, *Electron Paramagnetic Resonance in Compounds of Transition Elements* (Wiley, New York, 1974), Chap. 3.

[26] G. I. Malovichko, A. A. Karmazin, I. P. Bykov, V. V. Laguta, and V. P. Yarunichev, Fiz. Tverd. Tela (Leningrad) **25**, 3543 (1983) [Sov. Phys. Solid State **25**, 2038 (1983)].

[27] V. G. Grachev and G. I. Malovichko, Fiz. Tverd. Tela (Leningrad) **27**, 686 (1985) [Sov. Phys. Solid State **27**, 424 (1985)].

[28] A. Abraham and B. Bleaney, *Electron Paramagnetic Resonance of Transition Ions* (Clarendon, Oxford, 1970), Chap. 4.

[29] M. D. Glinchuk, V. G. Grachev, M. F. Deigen, A. B. Roitzin, and L. A. Suslin, *Electric Effects in Radiospectroscopy, Electron Paramagnetic, Electron Nuclear Double and Paraelectric Resonances* (Nauka, Moscow, 1981), Chap. 4.

[30] J.-M. Spaeth, J. R. Niklas, and R. H. Bartram, *Structural Analysis of Point Defects in Solids: an Introduction to Multiple Magnetic Resonance Spectroscopy* (Springer, Singapore, 1992), Chaps. 6 and 7.

[31] G. Malovichko, V. Grachev, A. Hofstaetter, E. Kokanyan, A. Scharmann, and O. Schirmer (unpublished).

[32] L. Kovacs, I. Földvari, I. Cravero, K. Polgar, and R. Capelletti, Phys. Lett. A **133**, 433 (1988).

[33] J. Diaz-Caro, J. Garsia-Sole, D. Bravo, T. P. J. Han, F. Jaque, and B. Henderson, Ferroelectr. Lett. Sect. **23**, 27 (1997).

[34] G. Corradi, H. Soethe, J.-M. Spaeth, and K. Polgar, J. Phys.: Condens. Matter **3**, 1901 (1991).

[35] G. Corradi, H. Soethe, J.-M. Spaeth, and K. Polgar, Ferroelectrics **125**, 295 (1992).

[36] O. Thiemann, G. Corradi, and H.-J. Reyher, Ferroelectrics **125**, 283 (1992).

[37] J. Diaz-Caro, J. Garsia-Sole, D. Bravo, J. A. Sanz-Garsia, F. J. Lopez, and F. Jaque, Phys. Rev. B **54**, 13 042 (1996).

[38] J. Diaz-Caro, J. Garsia-Sole, J. L. Martinez, B. Henderson, F. Jaque, and T. P. J. Han, Opt. Mater. **10**, 69 (1998).

[39] A. Martin, F. J. Lopez, and F. Agullo-Lopez, J. Phys.: Condens. Matter **4**, 847 (1992).

[40] G. A. Torchia, J. A. Sanz-Garsia, F. J. Lopez, D. Bravo, J. Garsia-Sole, F. Jaque, H. G. Gallagher, and T. P. J. Han, J. Phys.: Condens. Matter **10**, L341 (1998).

[41] D. Bravo, A, Martin, M. Voda, and F. J. Lopez, in *Abstracts of European Meeting ''Defects in Insulating Materials,'' 1994* (EURODIM-94, Lyon, France), p. 112.

[42] A. Kling, J. C. Soares, M. F. da Silva, J. A. Sanz-Garsia, E. Dieguez, and F. Agullo-Lopez, Nucl. Instrum. Methods Phys. Res. B **136–138**, 426 (1998).

[43] G. Malovichko, O. Cerclier, J. Estienne, V. Grachev, E. Kokanyan, and C. Boulesteix, J. Phys. Chem. Solids **56**, 1285 (1995).

[44] G. I. Malovichko, V. G. Grachev, and S. N. Lukin, Fiz. Tverd. Tela (Leningrad) **28**, 991 (1986) [Sov. Phys. Solid State **28**, 553 (1986)].

[45] G. I. Malovichko, V. G. Grachev, and V. V. Trotskii, Fiz. Tverd. Tela (Leningrad) **29**, 607 (1987) [Sov. Phys. Solid State **29**, 349 (1987)].

[46] G. G. Sia and Zhao Min-Guang, Phys. Rev. B **43**, 13 575 (1991).

[47] G. Malovichko, V. Grachev, and O. Schirmer, Ferroelectrics **185**, 639 (1996).